

Paleoceanography and Paleoclimatology

RESEARCH ARTICLE

10.1029/2019PA003774

Key Points:

- We compare core-top individual planktic foraminifera Mg/Ca temperatures to modern ocean temperatures in the equatorial Pacific
- Individual measurements of Mg/Ca in *G. ruber* and *N. dutertrei* retain site-specific temperature variability and differences between sites
- Mg/Ca individual foraminifera analysis is a valid tool for reconstructing past El Niño Southern Oscillation temperature variability

Supporting Information:

- Supporting Information S1

Correspondence to:

B. L. Rongstad,
brigitta.rongstad@colorado.edu

Citation:

Rongstad, B. L., Marchitto, T. M., Serrato Marks, G., Koutavas, A., Mekik, F., & Ravelo, A. C. (2020). Investigating ENSO-related temperature variability in equatorial Pacific core-tops using Mg/Ca in individual planktic foraminifera. *Paleoceanography and Paleoclimatology*, 35, e2019PA003774. <https://doi.org/10.1029/2019PA003774>

Received 20 SEP 2019

Accepted 22 NOV 2019

Accepted article online 26 NOV 2019

Investigating ENSO-Related Temperature Variability in Equatorial Pacific Core-Tops Using Mg/Ca in Individual Planktic Foraminifera

Brigitta L. Rongstad¹ , Thomas M. Marchitto¹ , Gabriela Serrato Marks² , Athanasios Koutavas³ , Figen Mekik⁴ , and Ana Christina Ravelo⁵

¹Department of Geological Sciences and Institute of Arctic and Alpine Research, University of Colorado Boulder, Boulder, CO, USA, ²Department of Earth, Atmospheric and Planetary Sciences, Massachusetts Institute of Technology, Cambridge, MA, USA, ³Department of Engineering Science and Physics, College of Staten Island, City University of New York, New York, NY, USA, ⁴Department of Geology, Grand Valley State University, Allendale, MI, USA, ⁵Department of Ocean Sciences and Institute of Marine Sciences, University of California, Santa Cruz, CA, USA

Abstract El Niño Southern Oscillation (ENSO) is the largest source of interannual climate variability on Earth today; however, future ENSO remains difficult to predict. Evaluation of paleo-ENSO may help improve our basic understanding of the phenomenon and help resolve discrepancies among models tasked with simulating future climate. Individual foraminifera analysis allows continuous down-core records of ENSO-related temperature variability through the construction and comparison of paleotemperature distributions; however, there has been little focus on calibrating this technique to modern conditions. Here, we present data from individual measurements of Mg/Ca in two species of planktic foraminifera, surface dwelling *Globigerinoides ruber* and thermocline dwelling *Neogloboquadrina dutertrei*, from nine core tops across the equatorial Pacific ($n \approx 70$ per core for each species). Population variance, kernel probability density functions, and quantile-quantile analyses are used to evaluate the shape of each Mg/Ca-temperature distribution and to compare them to modern conditions using monthly temperatures from the Simple Ocean Data Assimilation. We show that populations of individual Mg/Ca measurements in both *G. ruber* and *N. dutertrei* reflect site-specific temperature distribution shapes and variances across the equatorial Pacific when accounting for regional differences in depth habitats. Individual measurements of both taxa capture zonal increases in population variance from the western equatorial Pacific to the central equatorial Pacific and a spatially heterogeneous eastern equatorial Pacific, consistent with modern conditions. Lastly, we show that populations of individual Mg/Ca measurements are able to recover meaningful differences in temperature variability between sites within the eastern equatorial Pacific, lending support to this tool's application for paleo-ENSO reconstructions.

1. Introduction

El Niño Southern Oscillation (ENSO) is Earth's dominant mode of interannual climate variability. While initiated in the tropical Pacific, ENSO is responsible for widespread climatic, ecological, and societal impacts, including increased rain and flooding in coastal Ecuador and Peru and increased drought and fires in Indonesia during El Niño events. Despite the importance of ENSO for modern day climate variability and its impacts on communities around the globe, future ENSO remains difficult to predict. General circulation models used in recent Intergovernmental Panel on Climate Change (IPCC) reports are split among predictions of enhanced, reduced, or unchanged ENSO variability by the end of the 21st century (Collins et al., 2010; Meehl et al., 2007), and the IPCC reports *low confidence* in projections of future ENSO variability (Christensen et al., 2013). Reconstructions of paleo-ENSO may help resolve these discrepancies through improving our knowledge of its responses to past radiative and climatic forcings.

The interannual behavior of ENSO limits the archives from which ENSO can be reconstructed to those that are able to preserve short-term (monthly to annual) variability. Annually banded corals provide high-resolution records of past ENSO (e.g., Cobb et al., 2013; Hughen et al., 1999; Tudhope et al., 2001). However, long continuous records of past ENSO are difficult to reconstruct from individual corals. Annually varved lake sediments from the tropical Andes have also been used to reconstruct past ENSO

through evaluation of changes in precipitation and/or lake sedimentation (e.g., Moy et al., 2002; Rodbell et al., 1999). However, the nonlinear response of rainfall to sea surface temperatures (SSTs) in the equatorial Pacific (Emile-Geay & Tingley, 2016), specifically the difference in rainfall between Eastern Pacific and coastal El Niño events (extreme precipitation) and Central Pacific El Niño and La Niña events (less intense precipitation) (Kiefer & Karamperidou, 2019), makes it difficult to directly attribute changes in lake deposition to ENSO.

Individual foraminifera analysis (IFA), an emerging tool for reconstructing past ENSO (e.g., Ford et al., 2015; Khider et al., 2011; Koutavas et al., 2006; Koutavas & Joanides, 2012; Leduc et al., 2009; Rustic et al., 2015; Scroxton et al., 2011; White et al., 2018), allows the construction of long, continuous down-core records of monthly scale SST variability. While its utility has been tested in down-core applications, little focus has been placed on calibrating this method to modern conditions (Groeneveld et al., 2019). Here we ground truth a method for reconstructing temperature variability (seasonal plus interannual) using populations of individual Mg/Ca measurements in two species of planktic foraminifera, *Globigerinoides ruber* and *Neogloboquadrina dutertrei*. We compare these populations to temperature distributions simulated from the Simple Ocean Data Analysis (SODA) monthly temperatures. We compare variances and employ probability density functions (pdfs) and quantile-quantile (Q-Q) analysis to evaluate whether individual measurements of Mg/Ca in *G. ruber* and *N. dutertrei* accurately capture temperature variability at sites across the equatorial Pacific.

2. Individual Foraminifera Analysis

The theoretical framework for IFA is based on the observation that planktic foraminifera live on the order of 2–4 weeks (Spero, 1998), which is a short enough life span to capture monthly changes in ocean temperatures associated with ENSO. While the chemical analysis of a single sample containing multiple specimens of planktic foraminifera results in the averaging of individual calcification temperatures, the analysis of multiple samples each containing a single planktic foraminifer preserves population statistics that can be used to interpret changes in temperature variability.

Temperatures inferred from IFA, such as those calculated from $\delta^{18}\text{O}$ (Khider et al., 2011; Koutavas et al., 2006; Koutavas & Joanides, 2012; Leduc et al., 2009; Rustic et al., 2015; Scroxton et al., 2011) or Mg/Ca ratios (Ford et al., 2015; White et al., 2018), allow paleoceanographers to probe past changes in mean state, seasonality, and interannual (ENSO) variability. A change in the background mean state with no change in variance can be observed as a positive or negative shift in a temperature population (Figure 1a). In contrast, a change in seasonality or ENSO variability will theoretically affect the height and tails of a temperature distribution: An increase in variability will result in the shortening and broadening of a temperature distribution (Figure 1b), while a decrease in variability will result in a heightening and narrowing of a temperature distribution (Figure 1c). For ENSO, these changes assume a symmetric response of El Niño (warm) and La Niña (cold) events. In the eastern equatorial Pacific (EEP) and central equatorial Pacific (CEP), changes in ENSO variability may be more easily captured by the warm tails of IFA temperature populations because SST anomalies are greater during El Niño events than during La Niña events (An & Jin, 2001). Furthermore, site selection is important for disentangling total and ENSO variability because changes in seasonality can manifest as changes in temperature distribution shape similar to those predicted for ENSO (Thirumalai et al., 2013). For example, sites where ENSO has a larger impact than seasonality on modern temperature distributions have been targeted for diagnosing past changes in ENSO (Ford et al., 2015; White et al., 2018).

3. Materials and Methods

3.1. Sample Selection and Chemical Analysis

Samples were obtained from nine sediment core tops across the equatorial Pacific, including one site in the western equatorial Pacific (WEP), two sites near the Line Islands in the CEP, and six sites in the EEP (Figure 2 and Table 1). In order to evaluate differences in oceanographic regimes across the equatorial Pacific and within the EEP, core tops were selected to cover a range of modern total and interannual temperature variability, at both the sea surface and at depth (Figure 2). Total temperature variability was computed from SODA v.2.2.4 as the root mean square anomaly of monthly temperatures, and interannual

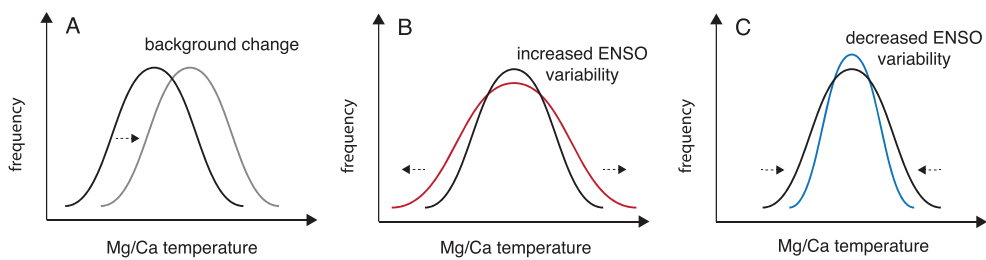


Figure 1. Theoretical models for interpreting changes in background state and ENSO using Mg/Ca-derived temperature distributions (adapted from Leduc et al., 2009 and Khider et al., 2011). (a) Changes in background state with no change in temperature variability. (b) Increased ENSO variability (red) results in a flattened temperature distribution and an increase in temperature variance. (c) Decreased ENSO variability (blue) results in a heightened temperature distribution and a decrease in temperature variance.

temperature variability was computed as the root mean square anomaly of monthly temperature anomalies (Figure 2).

Previous paleo-ENSO work suggests a shift in ENSO mean-state and variance between the mid-Holocene and late Holocene (Koutavas et al., 2006), so sampling was limited to sites with calibrated radiocarbon ages of approximately 4,500 years or younger (Table 1). Calibrated radiocarbon ages were previously reported for MGL1208-26MC (Costa et al., 2016), MGL1208-14MC (Costa et al., 2016; White et al., 2018), KNR195-5 MC-42A (Rustic et al., 2015), and RC13-140 and RC23-22 (Doss & Marchitto, 2013) (supporting information Table S1). We calibrated the raw radiocarbon dates previously presented in Berger and Killingley (1982) for Sites ERDC 92Bx and PLDS 72Bx using the MARINE13 calibration curve (Reimer et al., 2013) (Table S1). Two new radiocarbon ages were generated for KNR195-5 11-MCA and OC73-1-2 using specimens of *N.*

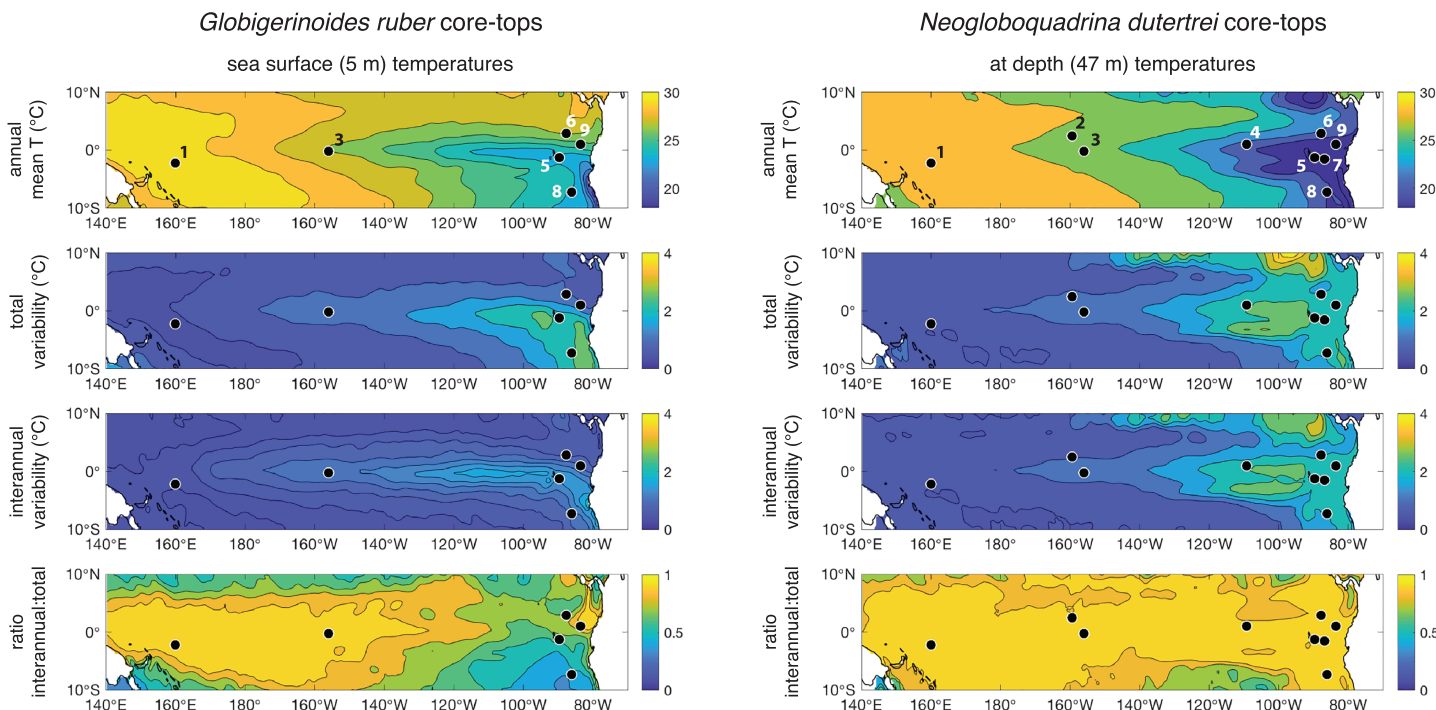


Figure 2. Core-top locations for *G. ruber* marked on modern sea surface temperature maps (left panels) and for *N. dutertrei* marked on modern 47 m temperature maps (right panels). Temperature maps are based on the Simple Ocean Data Analysis monthly temperatures v.2.2.4 for the Years 1981–2008. (top row) Mean annual temperatures. (second row) Root mean square anomaly of monthly temperatures, a measure of total variability (seasonality and ENSO). (third row) Root mean square anomaly of monthly temperature anomalies, a measure of interannual variability (ENSO). (bottom row) Ratio between (c) and (b), a measure of ENSO's contribution to total SST variability.

Table 1
Core-Top Information

Core	Water depth (m)	Depth in core (cm)	Radiocarbon age (years)	Calibrated radiocarbon age (years) ^a	Latitude	Longitude	<i>G. ruber</i> sample size	<i>N. dutertrei</i> sample size
(1) ERDC 92Bx	1,598	0–0.5	4,230 ± 240 ^b	4,039 ^c	2°13'S	156°59'E	69	69
(2) MGL 1208-26MC	3,545	0–1	3,900 ± 35 ^d	3,880 ^d	2°28'S	156°24'W	Too few	69
(3) MGL 1208-14MC	3,049	0–0.5	4,030 ± 40 ^e	4,030 ^e	0°13'S	155°58'W	72	68
(4) PLDS 72Bx	3,626	0–1	3,900 ± 70 ^b	3,728 ^c	1°1'N	109°16'W	Too few	73
(5) KNR195-5 MC-42A	615	5–5.5	805 ± 25 ^f	377 ^f	1°15'S	89°41'W	89	91
(6) RC13-140	2,246	0–5	1,750 ± 25 ^g	1,260 ^g	2°52'N	87°45'W	69	83
(7) KNR195-5 MC-11A	2,288	2–3	1,810 ± 15 ^c	1,251 ^c	1°32'S	86°47'W	Too few	69
(8) OC73-1-2	3,200	0–1	4,560 ± 15 ^c	4,516 ^c	7°17'S	86°37'W	74	68
(9) RC23-22	3,215	0–3	2,490 ± 20 ^g	2,020 ^g	1°N	83°37'W	57	66

^aDetailed information pertaining to calibrated radiocarbon ages, including ΔR values and accession numbers, are located in the supporting information text and in Table S1. ^bBerger and Killingley (1982). ^cThis study. ^dCosta et al. (2016). ^eWhite et al. (2018). ^fRustic et al. (2015). ^gDoss and Marchitto (2013).

dutertrei. Samples were graphitized at the University of Colorado and analyzed on an accelerator mass spectrometer at the University of California, Irvine, and converted to calendar ages using the MARINE13 calibration curve (Reimer et al., 2013) (Table S1).

Modern ENSO variability is exhibited in ocean temperatures both at the sea surface and at depth within the thermocline. In the thermocline, interannual variability accounts for most of the total variability because seasonality is largely restricted to the near surface, making the thermocline an appealing target for paleo-ENSO reconstruction (Figure 2). Therefore, two species of planktic foraminifera, surface dwelling *G. ruber* (250–355 μm) and thermocline dwelling *N. dutertrei* (355–425 μm), were selected for analyses. Morphotypes of both species were recorded prior to chemical cleaning but are not separated in our analyses to avoid potential bias toward a specific depth habitat or temperature range. At each site, approximately 70 individuals or greater of each species were picked and analyzed for Mg/Ca ratios (Table 1). The only site with less than ~70 specimens is Site RC23-22 which contains 57 individuals for *G. ruber*. Due to poor preservation, only a few specimens of *G. ruber* survived chemical cleaning at Site MGL1208-26MC in the CEP and at Sites PLDS 72Bx and KNR195-5 MC-11A in the EEP, so *G. ruber* Mg/Ca data are not presented for those cores. Individuals were oxidatively cleaned, dissolved, and analyzed by inductively coupled plasma mass spectrometry following procedures outlined in Rongstad et al. (2017), with analytical precision of ±0.6% on Mg/Ca (1σ). Al/Ca, Fe/Ca, and Mn/Ca were also measured to monitor for sedimentary contamination. Mg/Ca data from ERDC92Bx were presented previously by Rongstad et al. (2017).

3.2. Statistical Analysis of Inferred Temperatures

Planktic foraminiferal Mg/Ca is a well-established tool for reconstructing past ocean temperatures (e.g., Nürnberg et al., 1996; Lea et al., 1999; Elderfield & Ganssen, 2000; Anand et al., 2003). We model the foraminiferal Mg/Ca data in an inverse sense, converting Mg/Ca to calcification temperatures, because that is the task facing paleoceanographers; and because Mg/Ca-inferred temperature variability is insensitive to partial dissolution, in contrast to Mg/Ca variability (Rongstad et al., 2017). Inferred temperatures were calculated from Mg/Ca ratios using the Anand et al. (2003) sediment trap temperature calibrations, specifically their geometric mean method for *G. ruber* white (250–350 μm) giving a 10% increase in Mg/Ca per °C, and their assumed exponential constant method for *N. dutertrei* (350–500 μm) giving 9% per °C. Implications of using a lower temperature sensitivity for *G. ruber* (e.g., Gray et al., 2018) are discussed in section 4.3. In at least some species of planktic foraminifera, Mg/Ca is subject to small ancillary influences from salinity (3% to 5% per salinity unit) (Allen et al., 2016; Gray et al., 2018; Gray & Evans, 2019; Hönisch et al., 2013; Lea et al., 1999) and pH (−5% to −9% per 0.1 pH unit) (Gray et al., 2018; Gray & Evans, 2019) that are not modeled here but are discussed in section 4.3.

While partial dissolution results in a reduction of planktic foraminiferal Mg/Ca ratios (Brown & Elderfield, 1996; Dekens et al., 2002; Regenberg et al., 2014; Rosenthal & Lohmann, 2002), *G. ruber* and *N. dutertrei* lose Mg to partial dissolution as a percentage of the Mg initially present, resulting in no significant change in calculated temperature variance or temperature distribution shape (Rongstad et al., 2017). Therefore, a

dissolution correction scheme is unnecessary to evaluate differences or changes in temperature distributions derived from individual measurements of Mg/Ca in these taxa. Instead, we subtract the population's mean temperature from each of the individual temperatures, resulting in a modified population centered around zero that can be compared to similarly treated instrumental data. Note that population mean temperatures were cooler than the regional-habitat SODA simulations by an average of 2.5 °C (1.9 °C excluding RC13-140) for *G. ruber* and 5.6 °C for *N. dutertrei*, reflecting a cold bias probably due to partial dissolution.

Modern ocean temperatures for each site and depth were estimated using the monthly reanalysis (Years 1981–2008) from SODA v.2.2.4. In order to more directly compare the SODA temperatures to the temperatures derived from Mg/Ca in planktic foraminifera, theoretical distributions of Mg/Ca-based temperatures for *G. ruber* and *N. dutertrei* were simulated from SODA using a Monte Carlo approach. First, spatially uniform depth habitats were assumed for both *G. ruber* and *N. dutertrei* for all sites across the equatorial Pacific (Figure 3, top). The depth distribution for *G. ruber* was simulated by constructing a normal distribution of SODA depths with a mean of 5 m and a standard deviation of 1 depth step in SODA (~10–12 m in the upper 50 m of the water column). This normal distribution was then truncated at the surface so that no depths could be shallower than the shallowest observation in SODA (5 m). The resulting *G. ruber* depth distribution is skewed toward deeper depths with a mean depth of 9 m (Figure 3, top). *N. dutertrei*'s depth distribution was simulated by constructing a normal distribution of SODA depths with a mean of 47 m and a standard deviation of 1 depth step in SODA (~12–15 m).

The simulated uniform depth distributions of *G. ruber* and *N. dutertrei* described above are consistent with observations of both species' depth habitats. *G. ruber* typically lives in the upper 50 m of the water column (Fairbanks et al., 1982; Faul et al., 2000; Ravelo & Fairbanks, 1992), and *N. dutertrei* lives in the thermocline (Fairbanks & Wiebe, 1980; Field, 2004; Ravelo & Fairbanks, 1992; Sautter & Thunell, 1991) where it likely feeds on marine snow (Fehrenbacher et al., 2018). In the EEP, where the majority of our core-tops are located, 47 m places *N. dutertrei* in the mid-to-deep thermocline (Figure 3).

While spatially uniform depth distributions for *G. ruber* and *N. dutertrei* produced good results in the EEP, they underestimate the foraminiferal variance in the CEP and WEP (see section 4.1). Therefore, CEP and WEP depth distributions were altered to account for regional oceanographic differences and observed patterns in *G. ruber* and *N. dutertrei* depth habitats across the equatorial Pacific (see section 4.2). In the CEP, the mixed layer and thermocline are much deeper than in the EEP, so *G. ruber* and *N. dutertrei* depth distributions were simulated to be deeper and broader. While the depth distributions for *N. dutertrei* remained normal in shape, depth distributions for *G. ruber* were simulated to be more skewed in shape. *G. ruber* (mean = 57 m) was simulated to be uniform in concentration from the surface to the top of the thermocline (~83 m depth) and decreasing in concentration below that depth (Figure 3, bottom). *N. dutertrei* was simulated to have normally distributed concentrations centered about a mean of $130 \text{ m} \pm 16\text{--}22 \text{ m}$ (1 depth step in SODA) (Figure 3, bottom). In the WEP, the mixed layer and thermocline are deeper still, so *G. ruber* was deepened to a mean of 66 m with a concentration that is uniform until decreasing below ~100 m depth and *N. dutertrei* was deepened to a mean of $150 \text{ m} \pm 18\text{--}25 \text{ m}$ (1 depth step in SODA) (Figure 3, bottom).

For each species and site, theoretical Mg/Ca temperature distributions were built by randomly sampling 70 depths from the species' depth distribution and then randomly sampling a monthly temperature (1981–2008) for each of the 70 depths. Foraminifera were assumed to have an equal probability of living during any month of the year because, with the exception of site OC73-1-2, the seasonal cycle weakly affects the observed total temperature variability in the equatorial Pacific (Figure 2). Each simulated temperature was then randomly perturbed by $0 \pm 1.5^\circ\text{C}$ (1σ) to approximate the inherent uncertainty in the Mg/Ca thermometer (Sadekov et al., 2008). This process was repeated 10,000 times to capture stochastic variability among the theoretical distributions.

Variance was computed for the planktic foraminifera Mg/Ca temperature distributions and for each of the simulated Mg/Ca temperature distributions. To contrast individual sites against the basin-wide equatorial Pacific average, temperatures were combined over the grid 10°S to 10°N and 140°E to 90°W using the uniform depth distributions of *G. ruber* (mean depth = 9 m) and *N. dutertrei* (mean depth = 47 in the spreads and shapes of the temperature distributions were evaluated using kernel pdfs and Q-Q analysis. Kernel pdfs are a nonparametric tool used to approximate the shape of a distribution without assuming normality. Kernels were constructed for the foraminifera Mg/Ca temperature distributions and for each of the 10,000

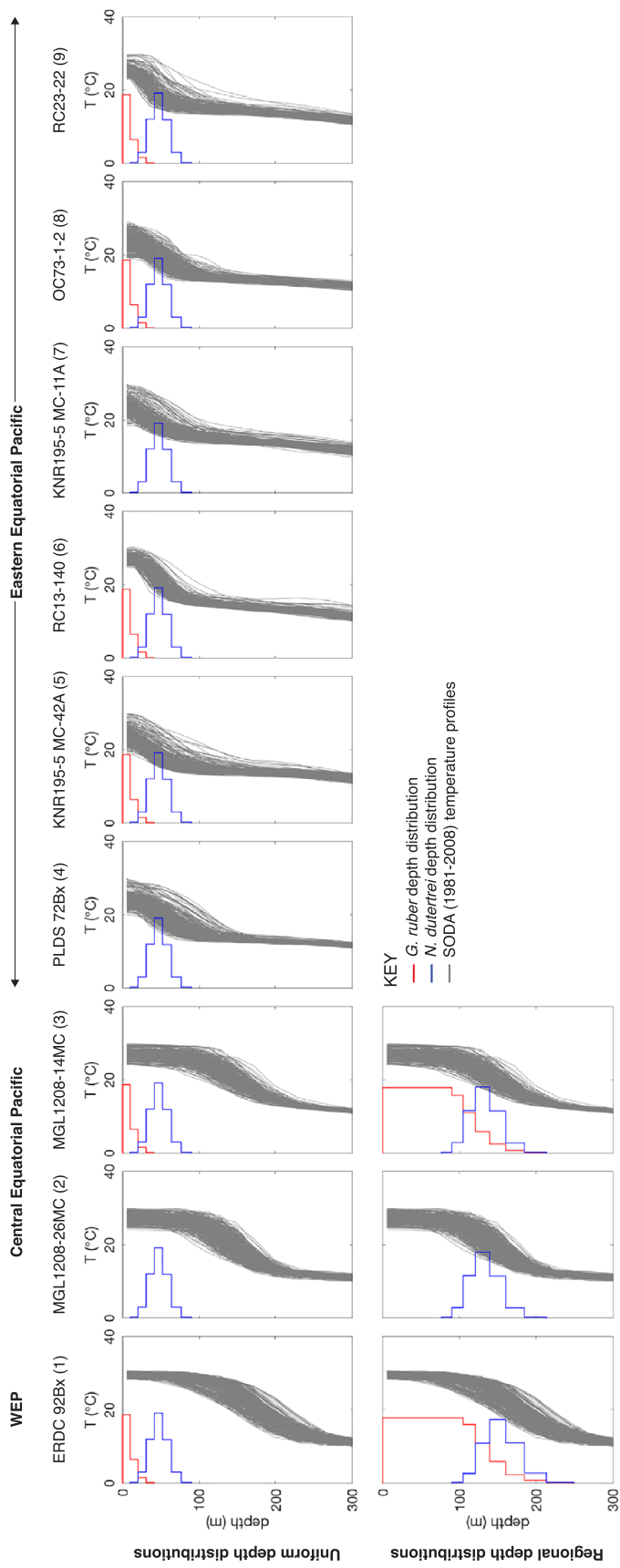


Figure 3. SODA v.2.2.4 (Years 1981–2008) monthly temperature profiles (gray lines) for each core-top location. The red histogram plots are the simulated *G. ruber* depth distributions, and the blue histogram plots are the simulated *N. dutertrei* depth distributions. Each bin is centered on a SODA depth. The width of the bins increase with depth to match the increase in distance between SODA depths from the surface to deep. (Top row) Simulated spatially uniform depth distributions for *G. ruber* (mean = 9 m) and *N. dutertrei* (mean = 47 m). (bottom row) Updated regional depth distributions for the WEP and the CEP. *G. ruber* depth distribution means are deepened to 66 and 57 m, respectively. *N. dutertrei* depth distribution means are deepened to 150 and 130 m, respectively.

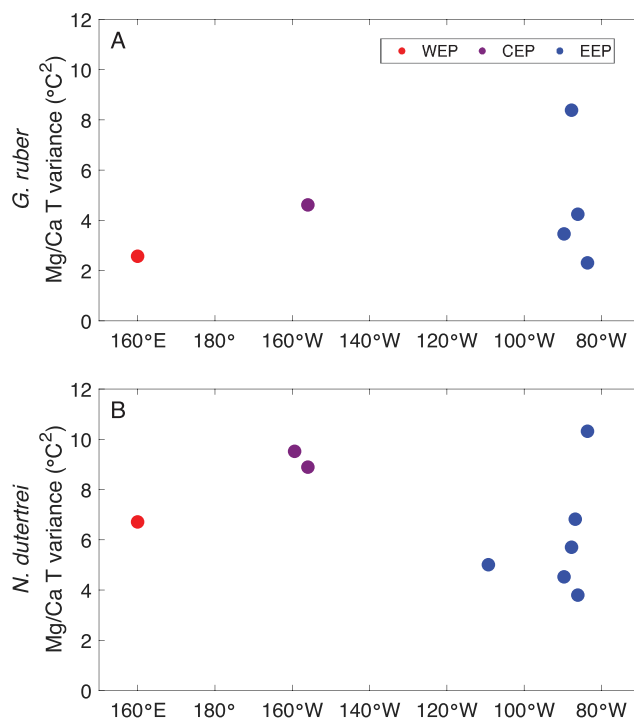


Figure 4. Scatter plots showing the computed planktic foraminifera Mg/Ca temperature variance across the equatorial Pacific for (a) the six *G. ruber* sites and (b) the nine *N. dutertrei* sites. Red filled circles are sites in the WEP, purple filled circles are sites in the CEP, and blue filled circles are sites in the EEP.

simulated SODA Mg/Ca temperature distributions at each site using the “fitdist” function in MATLAB (v.R2018b) and a bandwidth of 1. In order to test the fit of the foraminifera temperature kernels to the SODA temperature kernels, we computed the mean kernel and 95% confidence bounds using the temperature frequencies in each simulated kernel. A good fit between the temperature data sets is indicated when the foraminifera Mg/Ca temperature kernel falls within the 95% confidence bounds of the 10,000 simulated Mg/Ca temperature kernels.

Q-Q analysis is a powerful tool that highlights differences between distribution shapes by graphically comparing the quantiles of two populations (Wilks & Wilks & Gnanadesikan, 1968; Ford et al., 2015). Q-Q plots are used in this study in three ways: (1) to compare the shapes of the measured Mg/Ca temperature distributions to the simulated SODA Mg/Ca temperature distributions at each site, (2) to compare both the measured and simulated Mg/Ca temperature distributions at each site to basin-wide temperatures, to highlight site-specific or regional characteristics, and (3) to test the ability of Mg/Ca IFA to reconstruct hydrographic differences between sites. In order to test how well the planktic foraminifera Mg/Ca temperature distributions matched the simulated SODA Mg/Ca temperature distributions, a 95% confidence interval was calculated from the quantiles computed for each of the 10,000 simulated Mg/Ca temperature distributions. To estimate uncertainty when comparing measured (not simulated) Mg/Ca temperature distributions between two sites, a kernel pdf was fit to each distribution, and then 70 temperatures were resampled from each kernel 10,000 times. Quantiles were then computed for each of the 10,000 resamples, and confidence bounds (90% and 80%) were computed for each site by plotting the high bound quantiles of one location versus the low bound quantiles of the other location and vice versa.

4. Results and Discussion

Individual samples of *G. ruber* and *N. dutertrei* ($n = 1,186$) were picked and analyzed for Mg/Ca ratios. Of those samples, 42 (3.5%) were considered lost during cleaning (final mass $< 0.1 \mu\text{g CaCO}_3$), 34 (2.9%) were rejected due to having Al/Ca or Fe/Ca $\geq 1 \text{ mmol mol}^{-1}$ or Mn/Ca $\geq 1.5 \text{ mmol mol}^{-1}$, 17 (1.4%) were rejected due to having Mg/Ca $> 10 \text{ mmol mol}^{-1}$, and 9 (0.8%) were rejected for having inferred temperatures greater than 3 standard deviations above the means of their populations. The culled data set is therefore composed of 1,084 individuals.

Inspection of instrumental SSTs (Figure 2) leads us to expect that *G. ruber* Mg/Ca temperature distributions will exhibit a large range of intersite variances within the EEP, and a general increase in variance from the WEP, through the CEP, to the EEP average. Broadly speaking, this pattern is borne out in the *G. ruber* Mg/Ca observations: Variance in the WEP is less than both the variance in the CEP and the mean of the variances in the EEP (Figure 4a). The largest *G. ruber* variance is found in the EEP (Site RC13-140, variance = $8.4 \text{ }^{\circ}\text{C}^2$), and with the exception of the easternmost site (RC23-22), the smallest variance is found in the WEP (Site ERDC 92Bx, variance = $2.6 \text{ }^{\circ}\text{C}^2$).

Instrumental temperatures at 47 m (Figure 2) point toward a similar expectation for the zonal pattern of variance among *N. dutertrei* Mg/Ca temperature distributions. While *N. dutertrei* from the WEP indeed shows smaller Mg/Ca temperature variance than in the CEP, the EEP unexpectedly shows, on average, the smallest variance of all (Figure 4b). As discussed below, this observation can be explained by regional differences in depth habitats.

4.1. SODA Simulations With Uniform Depth Distributions

When assuming spatially uniform and shallow (mean = 9 m) depth habitats, the *G. ruber* Mg/Ca temperature distributions most closely match the simulations in the EEP (at three of four sites) (Figures 5a, 6, and 7).

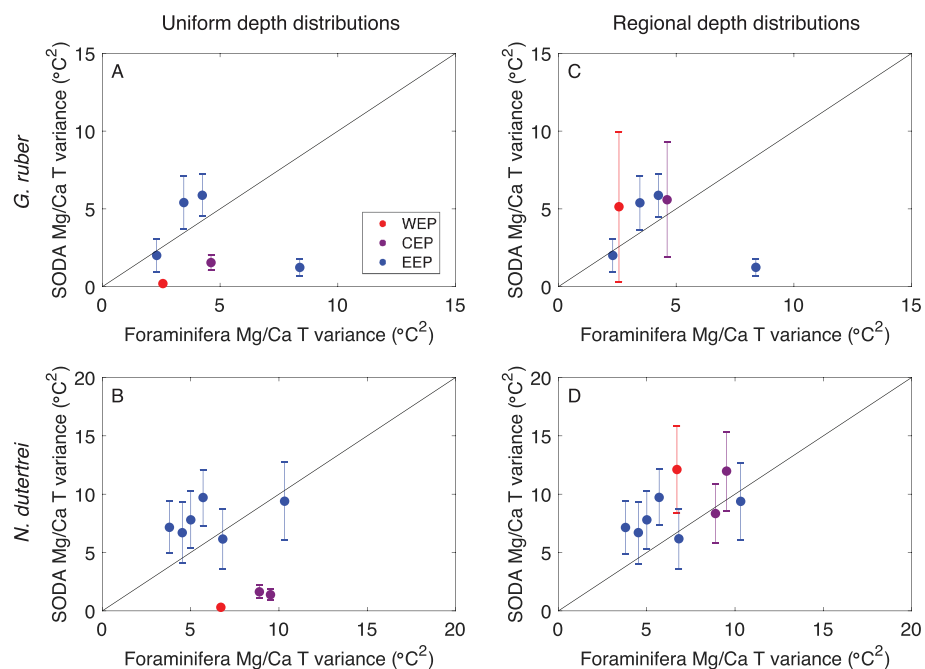


Figure 5. Scatter plots comparing the variance of the simulated SODA Mg/Ca temperature distributions (with 2 standard deviations of the 10,000 Monte Carlo simulations) to the *G. ruber* (a and c) and *N. dutertrei* (b and d) Mg/Ca temperature distributions. Uniform SODA depth distribution simulations are presented in (a) and (b). Regional SODA depth distribution simulations are presented in (c) and (d). Scatter points are color coded by region: WEP (red circles), CEP (purple circles), and EEP (blue circles). The outlier in the upper right panel is RC13-140.

Site RC23-22 in the EEP produces the best match: The quantiles of the measured temperature distribution fall mostly within the 95% confidence interval bounds of the simulated temperature distributions, and both measured and simulated temperature distributions exhibit normally distributed temperatures that are slightly smaller in spread than that of the basin-wide temperatures (Figure 7). At EEP Site OC73-1-2, there is a small divergence between the two data sets where the *G. ruber* temperature distribution does not capture the bimodal character of the SODA temperature simulations (Figure 6). At EEP Site KNR195-5 42-MCA, the *G. ruber* temperature distribution displays a slightly smaller warm tail than most of the SODA temperature simulations (Figure 6). However, despite these small divergences, the Q-Q plots for OC73-1-2 and KNR195-5-MC42A indicate that the quantiles of the *G. ruber* temperature distributions still fall mainly within the 95% confidence intervals of the 10,000 simulated SODA temperature distributions (Figure 7).

Larger divergences between *G. ruber* Mg/Ca temperatures and simulated temperatures occur in the WEP, CEP, and at Site RC13-140 in the EEP. At all three locations, the foraminifera Mg/Ca temperature distributions consistently produce a greater spread than the distributions simulated from SODA (Figures 5a, 6, and 7). Q-Q plots of *G. ruber* temperature distributions versus basin-wide temperatures fall almost entirely outside of the 95% confidence intervals of the 10,000 simulated SODA distributions (Figure 7), indicating poor matches for these three sites. At RC13-140, the *G. ruber* data exhibit a much longer warm tail than any of the SODA simulations (Figure 7).

The best matches between the shapes of the *N. dutertrei* temperature distributions and the uniform habitat (mean = 47 m) SODA temperature distributions, like *G. ruber*, occur in the EEP. There, the measured and simulated temperature distributions exhibit similar spreads (Figures 5c and 6), with the Q-Q plots at Sites RC23-22 and KNR195-5 11-MCA showing the strongest concordance between the measured and simulated temperatures (Figure 7). The *N. dutertrei* and simulated SODA temperature distributions at both sites, especially Site RC23-22, capture a distinct warm tail that is not found in the basin-wide temperatures (Figure 7). With the exception of RC13-140, the Q-Q plots of the remaining EEP sites also show close matches between the *N. dutertrei* and SODA temperature distributions. The *N. dutertrei* temperature distributions at EEP Sites

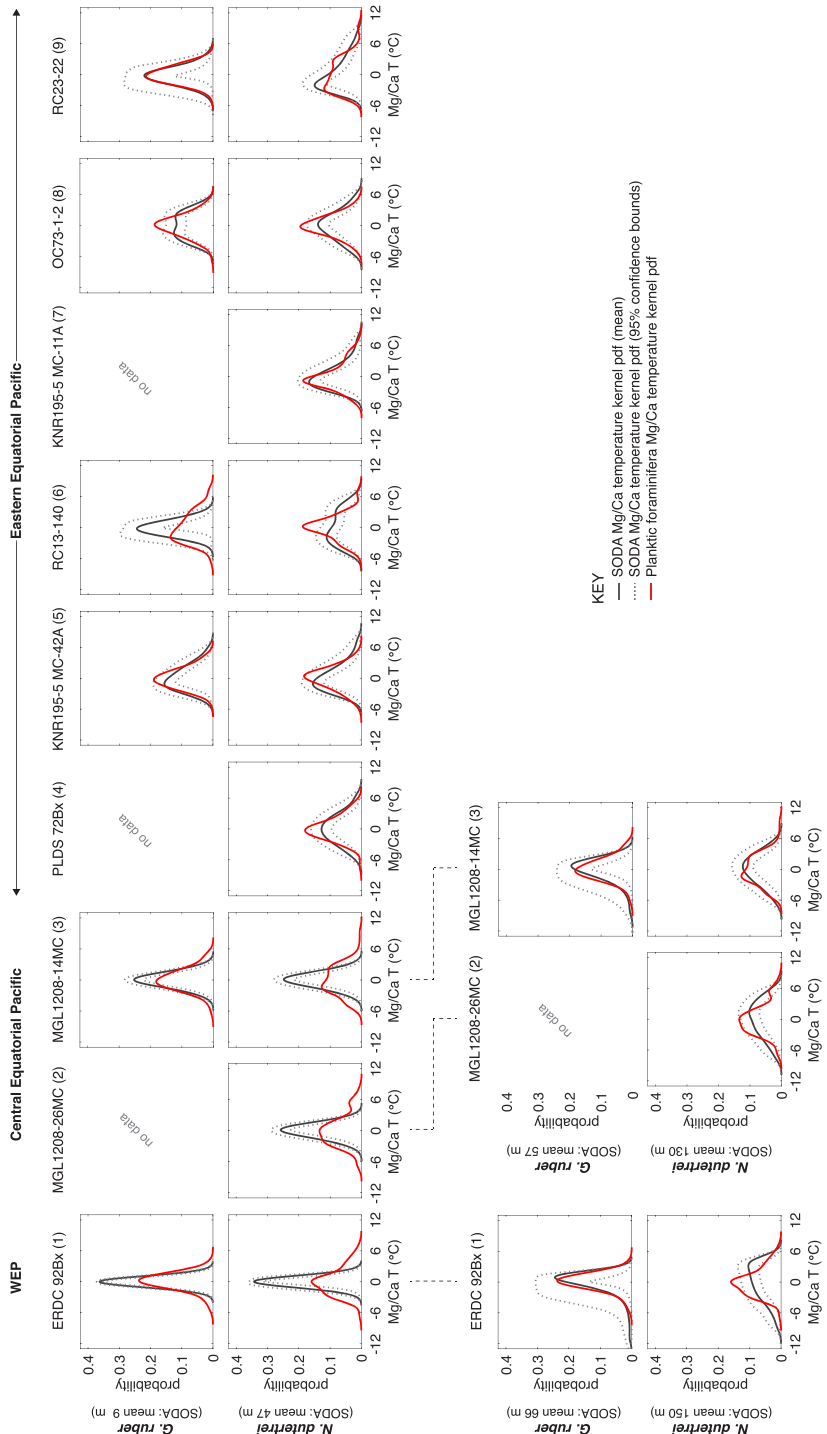


Figure 6. Kernel probability density functions for the *G. ruber* and *N. dutertrei* Mg/Ca temperature distributions (red) and for the simulated SODA Mg/Ca temperature distributions (dark gray). The solid gray line is the mean kernel of the 10,000 simulations, and the dotted gray lines are the 95% confidence bound kernels of the 10,000 simulations. A good match between the foraminifera and SODA Mg/Ca temperature distributions is indicated by the red kernel fitting within the 95% confidence bounds. All kernels are centered around zero. The kernels in the top two rows show the uniform depth SODA simulations, and the kernels in the bottom two rows show the regional depth SODA simulations for the WEP and CEP.

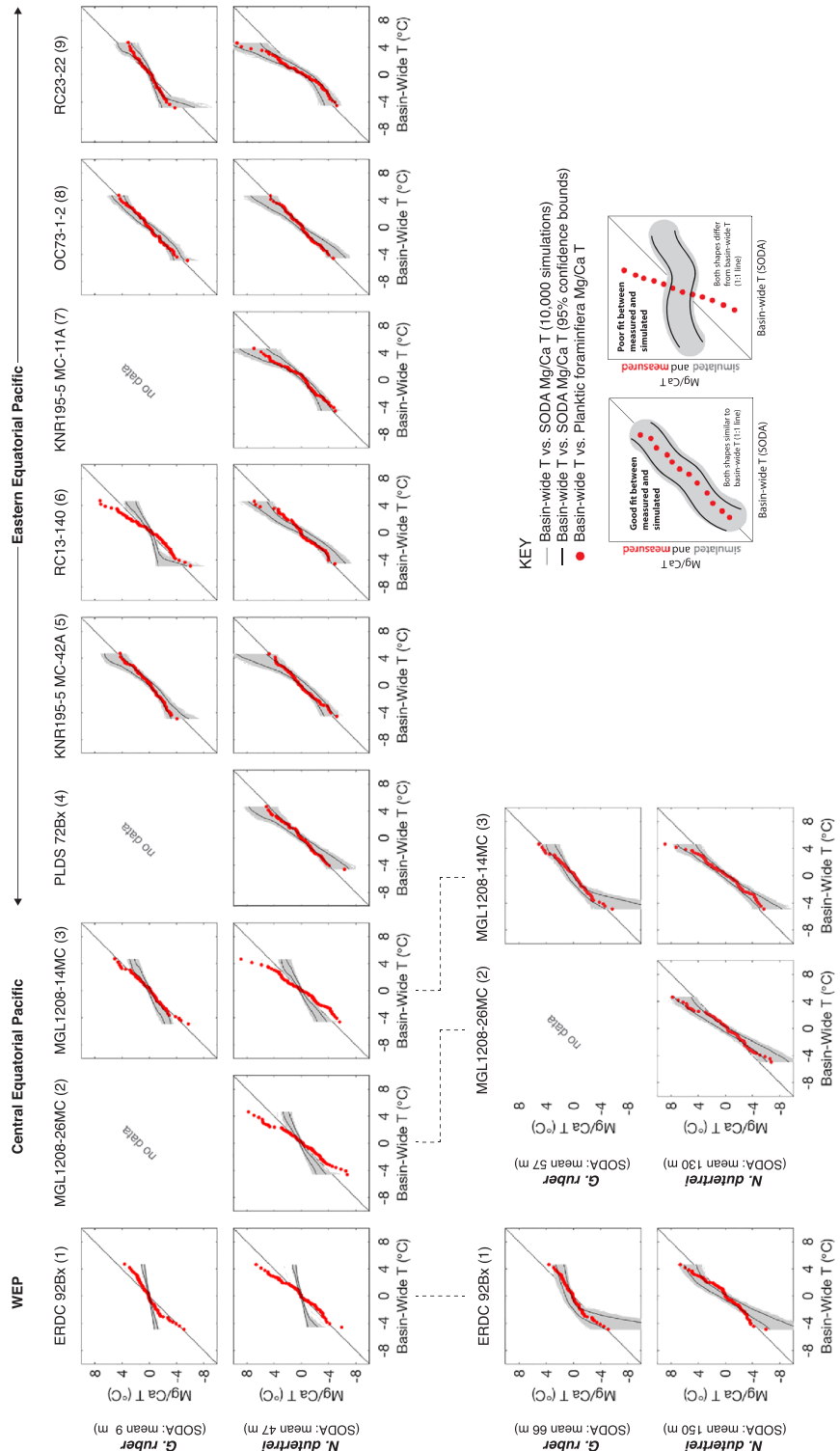


Figure 7. Q-Q plots comparing the foraminifera and simulated SODA Mg/Ca temperatures to basin-wide temperatures. The red quantiles show the comparison between the *G. ruber* and *N. dutertrei* Mg/Ca temperature distributions and basin-wide temperature distributions. The gray lines show the comparison between the 10,000 simulated SODA Mg/Ca temperature distributions and basin-wide temperature distributions. The black lines show the 95% confidence interval of the 10,000 simulated SODA Mg/Ca temperature distributions. A good match between foraminifera and simulated Mg/Ca temperature distributions is indicated by the red quantiles falling within the 95% confidence bounds. The top two rows show comparisons with uniform depth SODA simulations, and the bottom two rows show comparisons with regional depth SODA simulations for the WEP and CEP. In all cases, the basin-wide distributions are based on the uniform depths.

KNR195-5 MC-42A and PLDS 72Bx exhibit slightly smaller warm tails than predicted by the SODA simulations, and the *N. dutertrei* at OC73-1-2 exhibits a slightly narrower range of temperatures than the SODA temperature distributions (Figure 6). However, the Q-Q plots indicate an overall good fit between the two groups of data at each site (Figure 7).

Similar to the *G. ruber* data, the largest divergences between the *N. dutertrei* Mg/Ca temperature distributions and the simulated uniform-depth temperature distributions occur in the WEP, CEP, and at Site RC13-140 in the EEP. In the WEP and CEP, the *N. dutertrei* temperature distributions consistently produce temperature ranges that are greater than those simulated from SODA (Figures 5c and 6). The Q-Q plots of *N. dutertrei* temperature distributions versus basin-wide temperatures fall well outside of the 95% confidence interval bounds of the 10,000 SODA simulations, indicating large discordances between the two temperature groups (Figure 7). At Site RC13-140 in the EEP, the mismatch between the measured and simulated *N. dutertrei* Mg/Ca temperatures is not nearly as large, but the Q-Q plot does fall largely outside of the 95% confidence interval of the 10,000 simulations near the warm end of the distribution (Figure 7). In contrast to the *G. ruber* Mg/Ca at this site, *N. dutertrei* records less variance than the simulations, and the mismatch with SODA is less severe.

4.2. SODA Simulations With Regional Depth Distributions

Statistical tests indicate a high discordance between the foraminifera Mg/Ca temperature distributions and the uniform-depth SODA simulated Mg/Ca temperature distributions in the WEP and CEP (Figures 5–7). The observed discrepancies between measured and simulated Mg/Ca temperatures using shallow fixed depth habitats at our WEP site are mirrored by Groeneveld et al. (2019). In their western Pacific warm pool core top, the authors found that the standard deviations of their measured Mg/Ca temperatures were higher than predicted for *Trilobatus sacculifer* (assumed habitat = 35 m) and *N. dutertrei* (100 m), and they found little improvement in the discrepancy when expanding each species' depth habitat to a range (*T. sacculifer* = 20–70 m and *N. dutertrei* = 80–120 m) (Groeneveld et al., 2019). As the oceanographic regimes of the WEP, CEP, and EEP are different, these results are not surprising. The equatorial Pacific exhibits a zonally tilted thermocline, which is deep in the WEP and shallow in the EEP. This results in a much deeper mixed layer in the WEP, which combined with lower productivity allows warm water and light (important for photosymbionts) to penetrate much deeper than in the east. These differences have important implications for the depth habitats of planktic foraminifera.

G. ruber inhabits the mixed layer and is typically thought to live in the upper 50 m of the water column (Fairbanks et al., 1982; Faul et al., 2000; Ravelo & Fairbanks, 1992), but its peak calcification depth has been found to vary by region. In the EEP, its habitat depth is close to the sea surface due to a shallow thermocline and mixed layer. However, in the WEP, its peak calcification depth appears to be much deeper (50–100 m) based on geochemical comparisons between living planktic foraminifera and modern ocean water chemistry (Rippert et al., 2016). In the EEP, *N. dutertrei*'s average depth habitat is estimated to fall between 65 and 75 m as calculated by comparing core-top temperatures derived from $\delta^{18}\text{O}_{\text{calcite}}$ to modern temperatures recorded in GLODAP v1.1 (Mekik, 2018). In the WEP, comparisons of foraminiferal geochemistry to modern water chemistry suggest *N. dutertrei* has a mean calcification depth of 140 m (Rippert et al., 2016), and analysis of intrashell Mg/Ca variability suggests that the bulk of *N. dutertrei*'s test is built at the depth of the modern thermocline (~100–250 m) (Eggers et al., 2003). In the tropical Atlantic, $\delta^{18}\text{O}_{\text{calcite}}$ likewise indicates that *N. dutertrei* follows the thermocline, shoaling from ~100–150 m in the west to ~50–100 m in the east (Ravelo & Andreasen, 1999; Steph et al., 2009).

Accounting for deeper habitats for both *G. ruber* and *N. dutertrei* in the CEP and WEP would broaden the distributions of the SODA simulations there, potentially bringing them into closer agreement with the Mg/Ca observations. Regional depth corrections for the CEP and WEP were chosen by incorporating documented regional differences in habitat depth as described above. The *G. ruber* depth distributions were deepened to a mean of 57 m in the CEP and 66 m in the WEP, while the *N. dutertrei* depth distributions were deepened to a mean of 130 m in the CEP and 150 m in the WEP (see section 3.2 and Figure 3).

While they did not employ deeper habitats for their western Pacific warm pool site, Groeneveld et al. (2019) concluded that regional differences in depth habitat must be considered when interpreting temperature variability derived from individual measurements of Mg/Ca individual planktic foraminifera, and our

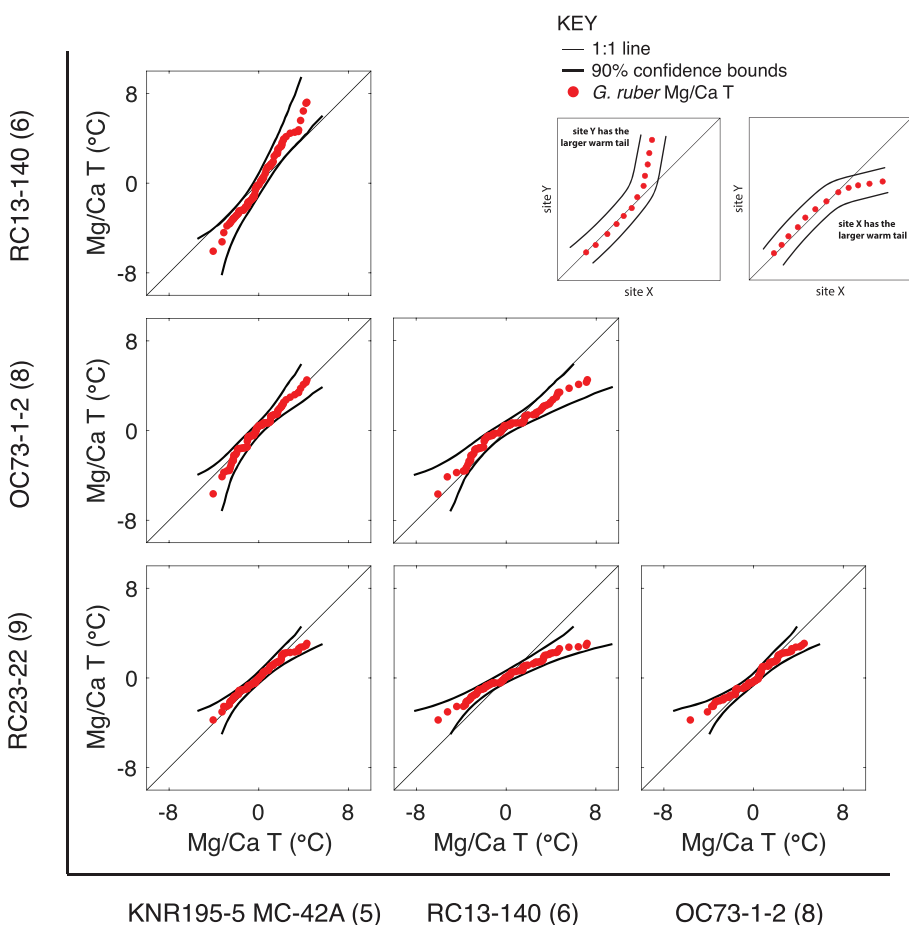


Figure 8. Matrix of Q-Q plots comparing the quantiles of the *G. ruber* Mg/Ca temperature distributions from within the EEP. The red points show the Q-Q plot comparing two sites. The bold black lines are the 90% confidence bounds which are used to estimate uncertainty in similarities and differences between sites. The straight black line is a 1:1 line. Two temperature distributions are significantly different (at the 90% confidence level) if the 1:1 line plots outside of the confidence bounds at any point.

results confirm their observation. Regional depth corrections dramatically improve concordance of both spread (Figures 5b, 5d, and 6) and shape (Figure 7) of the foraminifera and simulated Mg/Ca temperature distributions. The CEP and WEP planktic foraminifera temperature quantiles fall within the 95% confidence interval bounds of the 10,000 SODA temperature distribution simulations much more frequently than the simulations that employ a uniform-depth distribution (Figure 7). At Site ERDC92Bx in the WEP, the *G. ruber* and SODA simulated Mg/Ca temperature distributions both capture a distinct cold tail, though the *N. dutertrei* temperature distribution does not closely resemble the skewed shape of the simulated Mg/Ca temperature distribution (Figures 6 and 7). In the CEP, the *N. dutertrei* temperature distribution at Site MGL1208-26MC is still more abnormally shaped than the simulated SODA temperature distributions (Figure 6); however, Q-Q analysis shows a decent match between the foraminifera and simulated temperature distributions, with some quantiles falling outside the confidence bounds near the center of the temperature distributions (Figure 7). At Site MGL1208-14MC in the CEP, the quantiles for measured *G. ruber* temperatures fall much closer the 95% confidence bounds than the simulations using a uniform depth distribution but do also exhibit a longer warm tail than simulated (Figures 6 and 7). The quantiles for the measured *N. dutertrei* temperatures at this site fall mainly with the 95% confidence interval bounds of the 10,000 SODA simulations (Figures 6 and 7).

While our simulations assume foraminifera have an equal probability of living throughout the year, sediment trap studies in Panama Basin suggest that some species of planktic foraminifera exhibit their largest fluxes during the summer months or upwelling season (e.g., Bé et al., 1985; Thunell et al., 1983; Thunell

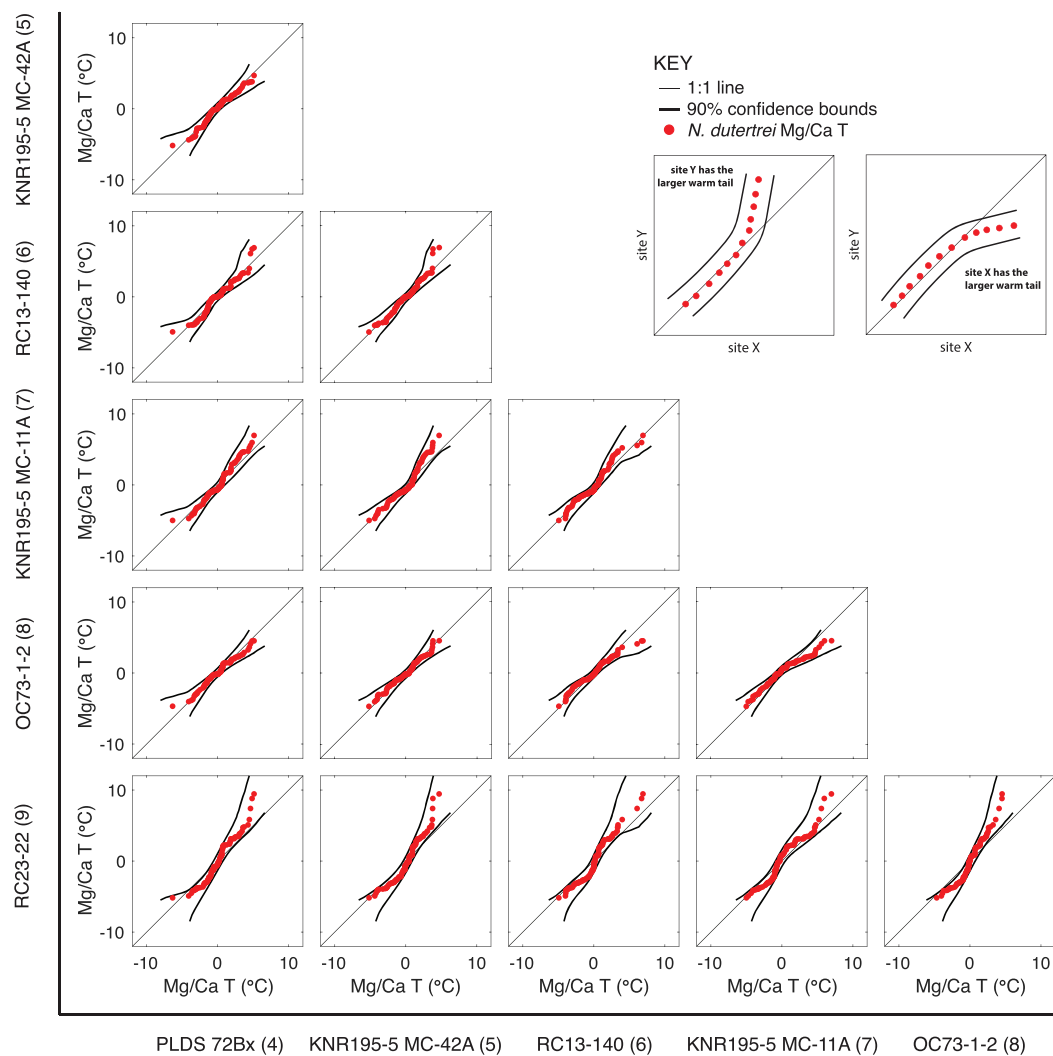


Figure 9. Matrix of Q-Q plots comparing the quantiles of the *N. dutertrei* Mg/Ca temperature distributions from within the EEP. The red points show the Q-Q plot comparing two sites. The bold black lines are the 90% confidence bounds which are used to estimate uncertainty in similarities and differences between sites. The straight black line is a 1:1 line. Two temperature distributions are significantly different (at the 90% confidence level) if the 1:1 line plots outside of the confidence bounds at any point.

& Reynolds, 1984). However, total temperature variability at most of our sites is dominated by interannual variability, with little seasonality (Figure 2), so repeating our simulations using particular seasons has negligible impact. Only one of our sites is dominated by the seasonal cycle (surface temperatures at OC73-1-2), but its location (7°S) makes it difficult to directly compare to the Panama Basin studies. We tested multiple seasonal flux scenarios in our SODA simulations of Mg/Ca temperature at OC73-1-2, but none of the scenarios are capable of improving the discrepancy between *G. ruber* and simulated Mg/Ca temperatures at both the warmest and coldest quantiles of the distributions.

The remaining discrepancies between the planktic foraminifera Mg/Ca temperature distributions and the simulated temperature distributions could be in part due to sampling errors. For example, the irregular shape of the *N. dutertrei* population at MGL1208-26MC (Figure 6) could possibly be improved with more Mg/Ca analyses. Other discrepancies, such as at Site RC13-140 where the *G. ruber* simulation is too narrow or OC73-1-2 where it is too broad (Figure 6), might be due to slight differences in depth habitat not accounted for in our selected depth distributions. Furthermore, it is possible that SODA temperatures do not capture the full range of variability experienced during the past few hundred to few thousand years that the foraminifera represent, and such a bias could vary by site.

4.3. Temperature Sensitivity, Salinity, and pH

While partial dissolution can be ruled out as a possible statistic modifier (Rongstad et al., 2017), the shapes of temperature distributions do rely partly on the choice of Mg/Ca temperature calibration. There is longstanding support for temperature sensitivities of ~8–10% Mg/Ca per °C, across multiple species of planktic foraminifera (e.g., Anand et al., 2003; Elderfield & Ganssen, 2000; Lea et al., 1999; Nürnberg et al., 1996). However, recent multivariate analyses of sediment trap data (Gray et al., 2018) and culture experiments (Gray & Evans, 2019) suggest that the Mg/Ca temperature sensitivity of *G. ruber* may actually be closer to 6%, with salinity and pH explaining significant portions of the Mg/Ca signal. A lower temperature sensitivity for *G. ruber* would broaden our inferred temperature distributions derived from Mg/Ca ratios, requiring broader depth distributions in the SODA simulations. However, since our approach does not include the effects of salinity and pH, which likely contribute to the observed Mg/Ca variance, that inferred temperature spread would be an overestimate. An explicit forward model of our Mg/Ca data using oceanographic observations of temperature, salinity, and pH is left to future work, but we make some preliminary observations below.

Total variability in salinity is relatively low for our equatorial Pacific core-top locations (<0.6 psu at the surface and <0.4 psu at 47 m depth) and is similar between sites (Giese & Ray, 2011), so it is unlikely that salinity is contributing significantly to either the measured Mg/Ca temperature variability or the differences in variability between our core-top locations. Furthermore, the similarity in salinity (both in annual and total variability) between Sites RC13-140 and RC23-22 cannot explain why the measured Mg/Ca temperatures at RC13-140 diverge from the simulated Mg/Ca temperatures while the measured Mg/Ca temperatures at RC23-22 closely match the simulated Mg/Ca temperatures.

The apparent temperature sensitivity of *G. ruber* Mg/Ca has recently been parsed into a “direct” thermal effect of ~6% per °C plus a pH effect that contributes another ~3% per °C, via the temperature sensitivity of the dissociation constant of water (i.e., higher temperature lowers pH, thereby boosting Mg/Ca) (Gray et al., 2018; Gray & Evans, 2019). To the extent that equatorial Pacific pH variability is controlled by the dissociation constant of water, the Anand et al. (2003) temperature sensitivity should adequately account for the combined influences of temperature and pH. However, cold and low-pH (carbon-rich) waters may be brought to the sea surface by upwelling, especially in the EEP (Key et al., 2015). Under such conditions, the direct thermal and pH influences on Mg/Ca may work in partial opposition, theoretically resulting in lower Mg/Ca variance. Total variability in sea surface pH ranges from ~0.01 to 0.03 pH units for our core-top locations, with maximum variance in the cold tongue east of Galapagos (Iida et al., 2015; Takatani et al., 2014). In terms of Mg/Ca, this pH variability should have a much smaller impact than temperature, but it also implies that pH and temperature are not strongly additive in the equatorial Pacific. Hence, a lower temperature sensitivity (Gray et al., 2018; Gray & Evans, 2019) may be appropriate.

4.4. EEP Site Comparisons

Comparisons of the foraminifera and simulated SODA Mg/Ca temperature distributions across the equatorial Pacific indicate that individual measurements of Mg/Ca in *G. ruber* and *N. dutertrei* are able to capture realistic site-specific temperature variability. However, to validate the utility of Mg/Ca IFA as a paleoceanographic proxy, it is also important to test whether it is able to capture differences in variability between sites. To do this, we used pairwise Q-Q analysis to compare observed Mg/Ca temperature distributions amongst all sites within the EEP, spanning a range of annual mean temperature, total temperature variability, and interannual temperature variability (Figure 2).

The measured Mg/Ca temperature distribution from Site RC13-140 exhibits a larger warm tail than any of the other *G. ruber* sites in the EEP at the 90% confidence level (very likely, by IPCC convention) (Figure 8). However, the depth distribution for *G. ruber* at Site RC13-140 does not produce a good match with SODA simulations of temperature and therefore may be capturing variability in Mg/Ca unrelated to temperature and/or temperature variability not captured in the SODA data set. The remaining EEP sites are more similar to each other in shape at the 90% confidence level (Figure 8). The *G. ruber* temperature distribution at Site RC23-22 exhibits a smaller range of temperatures than Sites KNR195-5 MC-42A and OC73-1-2 (Figure 8), which is consistent with SODA computations of total variability (Figure 2), but not statistically significant.

For *N. dutertrei*, Site RC23-22 exhibits a warm tail that is larger than at Sites PLDS 72Bx, KNR195-5 MC-42A, and OC73-1-2 at the 90% confidence level (Figure 9). Site KNR195-5 MC-11A *N. dutertrei* exhibits a larger warm tail than at Sites KNR195-5 MC-42A and OC73-1-2 at the 80% (likely) confidence level (Figure S3). These observations are corroborated by the SODA computations at 47 m: Both RC23-22 and KNR195 MC-11A are situated well within the region of relatively high interannual variability (the highest targeted in this study) (Figure 2), where El Niño events give the temperature distribution a distinct warm tail (Figure 6).

The easternmost EEP site (RC23-22) and the southernmost EEP site (OC73-1-2) provide valuable insight into the capability of Mg/Ca IFA to distinguish between sites with observable differences in hydrographic conditions. At the sea surface, Site OC73-1-2 experiences higher seasonality and total variability compared to Site RC23-22 as computed from SODA (Figure 2). The Q-Q plot comparing the *G. ruber* Mg/Ca temperature distributions indicates that the total temperature range of OC73-1-2 is the larger of the two sites (Figure 8) and corroborates the SODA computations. At 47 m depth, Site RC23-22 sits within a region of relatively high total and interannual variability, while Site OC73-1-2 sits on the boundary with a region of lower variability (Figure 2). This is corroborated by the Q-Q plot comparing the *N. dutertrei* Mg/Ca temperature distributions, which shows an elongated warm tail (attributable to ENSO variability) at Site RC23-22. Thus, the foraminifera correctly reconstruct which site is more variable at the surface and which site is more variable at depth.

4.5. Implications for Paleo-ENSO Reconstruction

Paleoceanographers often assume that planktic foraminiferal habitat depths remain constant through time. In this study, we inferred that *G. ruber* and *N. dutertrei* depths vary regionally, which raises the probability that they vary temporally. For reconstructing ENSO variability, this may actually be an advantage. As the mean depth of the thermocline changes with time, the most variable portion of the temperature profile could be pushed into or out of the habitat of foraminifera that hypothetically live within a constant depth range, producing a change in Mg/Ca variance that could be mistaken for a change in ENSO (Ford et al., 2015, 2018). In contrast, we suggest that *N. dutertrei* tracks the average depth of the thermocline, so that any past change in its Mg/Ca variance would be attributable to a change in temperature variance within the thermocline and hence most likely to a change in ENSO. Since ENSO itself involves an interannual change in the depth of the thermocline, this framework assumes that *N. dutertrei* does not inhabit a very narrow and specific portion of the thermocline but rather a range of depths that encompass its average position.

Selecting sites that accurately record changes in temperature variability is critical for paleo-ENSO reconstructions. Sites targeted for down-core work should exhibit a robust calibration based on coherence of core-top foraminifera Mg/Ca temperatures and modern ocean temperatures. Our results indicate there is an overall good match between the temperature data sets after accounting for differences in hydrographic regimes between regions, with occasional exceptions like RC13-140 *G. ruber* (Figures 6 and 7). Furthermore, sites selected for down-core work should exhibit modern interannual temperature variability and a high ratio of interannual to total temperature variability, so that past changes in seasonality are less likely to be mistaken for ENSO (Thirumalai et al., 2013). The latter qualification is likely more critical for *G. ruber* (surface) reconstructions where interannual temperature variability is smaller, and the seasonal cycle is larger, than what is observed at depth. Temperature maps derived from SODA highlight distinct differences between locations and depths across the equatorial Pacific. For example, the highest observed interannual variability occurs at depth (~47–70 m) (Figures 2 and S1), but regions of high interannual to total temperature variability do occur at the surface (Figure 2).

Groeneveld et al. (2019) suggest that ecology, including seasonal fluxes of foraminifera, may dramatically impact the spread of Mg/Ca and $\delta^{18}\text{O}$ temperatures. However, our analysis of simulated and measured Mg/Ca temperatures suggests that seasonal fluxes of foraminifera only results in a bias in locations dominated by seasonal temperature variability (Site OC73-1-2). Site selection for down-core work should therefore carefully consider simulations of temperature and/or proxy variability (e.g., Zhu et al., 2017) that highlight changes in seasonality.

Among the sites we analyzed, Site RC23-22 provides one of the best fits between the foraminifera and simulated SODA Mg/Ca temperature distributions (Figures 6 and 7) and exhibits both the largest ratio of

interannual to total variability at the surface and the largest observed interannual temperature variability at 47 m depth (Figure 2). The match between the temperature data sets for *G. ruber* is the best among all equatorial Pacific sites (Figure 7) and the measured temperature distribution exhibits the smallest warm tail in the EEP (Figure 8). The *N. dutertrei* temperature distribution at Site RC23-22 is an excellent match for the simulated SODA Mg/Ca temperature distribution and exhibits the largest warm tail of all the *N. dutertrei* temperature distributions in the EEP (Figure 8) and across the equatorial Pacific (Figure 7). Importantly, the elongated warm tail of the *N. dutertrei* Mg/Ca temperature distribution indicates that this may be an excellent site for capturing changes in variability in the warm tail (El Niño) in the past. While Site KNR195-5 MC-11A does not have *G. ruber* Mg/Ca temperatures to compare to simulations, it also exhibits a good match between the *N. dutertrei* temperature distribution and corresponding SODA simulations and is located within a region of relatively high interannual variability. Similar to Site RC23-22, the characteristic warm tail indicates that this site exhibits large warm temperature variability likely diagnostic of ENSO (El Niño) variance in the past.

5. Conclusions

We compared temperature distributions derived from individual measurements of Mg/Ca in *G. ruber* and *N. dutertrei* from nine core tops across the equatorial Pacific to temperature distributions simulated for the same locations using SODA. Our data show that populations of individual Mg/Ca measurements capture site-specific temperature distribution shapes and variance when accounting for regional differences in depth habitats across the equatorial Pacific. Populations of individual Mg/Ca measurements are able to recover differences in temperature variability between sites within the EEP, with some sites displaying distinct warm tails characteristic of El Niño events. This work demonstrates that Mg/Ca IFA is a valid tool for probing past ENSO variability, especially when targeting sites with substantial modern interannual temperature variability and a high ratio of interannual to total temperature variability.

Acknowledgments

We thank Payton Birdsong for assistance with picking specimens of foraminifera, John Morton for assistance with analysis on the ICP-MS, Dr. Kris Karnauskas for help with SODA computations, and Dr. Jennifer Hertzberg and an anonymous reviewer for their constructive reviews. This work was supported by National Science Foundation Grant OCE-1603023 to T. M. M. Core-top samples were provided by the Oregon State University Marine Geology Repository ([OCE-1558679](#)), WHOI Seafloor Samples Laboratory, and Lamont-Doherty Core Repository. Data presented in this paper are archived with the NCDC NOAA World Data Center for Paleoclimatology (<https://www.ncdc.noaa.gov/paleo/study/28335>).

References

- Allen, K. A., Hönnisch, B., Eggins, S. M., Haynes, L. L., Rosenthal, Y., & Yu, J. (2016). Trace element proxies for surface ocean conditions: A synthesis of culture calibrations with planktic foraminifera. *Geochimica et Cosmochimica Acta*, 193, 197–221. <https://doi.org/10.1016/j.gca.2016.08.015>
- An, S. I., & Jin, F. F. (2001). Collective role of thermocline and zonal advective feedbacks in the ENSO mode. *Journal of Climate*, 14, 3421–3432. [https://doi.org/10.1175/1520-0442\(2001\)014<3421:CROTAZ>2.0.CO;2](https://doi.org/10.1175/1520-0442(2001)014<3421:CROTAZ>2.0.CO;2)
- Anand, P., Elderfield, H., & Conte, M. H. (2003). Calibration of Mg/Ca thermometry in planktonic foraminifera from a sediment trap time series. *Paleoceanography*, 18(2), 1050. <https://doi.org/10.1029/2002PA000846>
- Bé, A. W., Bishop, J. K., Sverdrup, M. S., & Gardner, W. D. (1985). Standing stock, vertical distribution and flux of planktonic foraminifera in the Panama Basin. *Marine Micropaleontology*, 9(4), 307–333. [https://doi.org/10.1016/0377-8398\(85\)90002-7](https://doi.org/10.1016/0377-8398(85)90002-7)
- Berger, W. H., & Killingley, J. S. (1982). Box cores from the equatorial Pacific: ^{14}C sedimentation rates and benthic mixing. *Marine Geology*, 45(1–2), 93–125. [https://doi.org/10.1016/0025-3227\(82\)90182-7](https://doi.org/10.1016/0025-3227(82)90182-7)
- Brown, J., & Elderfield, H. (1996). Variations in Mg/Ca and Sr/Ca ratios of planktonic foraminifera caused by postdepositional dissolution: Evidence of shallow Mg-dependent dissolution preferentially. *Paleoceanography*, 11(5), 543–551. <https://doi.org/10.1029/96PA01491>
- Christensen, J. H., Krishna Kumar, K., Aldrian, E., An, S.-I., Cavalcanti, I. F. A., de Castro, M., et al. (2013). Climate phenomena and their relevance for future regional climate change. In T. F. Stocker, D. Qin, G.-K. Plattner, M. Tignor, S. K. Allen, J. Boschung, A. Nauels, Y. Xia, V. Bex, & P. M. Midgley (Eds.), *Climate change 2013: The physical science basis Contribution of Working Group I to the Fifth Assessment Report of the Intergovernmental Panel on Climate Change* (pp. 1217–1308). Cambridge, United Kingdom and New York: Cambridge University Press.
- Cobb, K., Westphal, N., Sayani, H., Watson, J., Di Lorenzo, E., Cheng, H., et al. (2013). Oscillation throughout the Holocene. *Science*, 339(6115), 67–70. <https://doi.org/10.1126/science.1228246>
- Collins, M., An, S. I., Cai, W., Ganachaud, A., Guilyardi, E., Jin, F. F., et al. (2010). The impact of global warming on the tropical Pacific Ocean and El Niño. *Nature Geoscience*, 3, 391–397. <https://doi.org/10.1038/ngeo868>
- Costa, K. M., McManus, J. F., Anderson, R. F., Ren, H., Sigman, D. M., Winckler, G., et al. (2016). No iron fertilization in the equatorial Pacific Ocean during the last ice age. *Nature*, 529(7587), 519–522. <https://doi.org/10.1038/nature16453>
- Dekens, P. S., Lea, D. W., Pak, D. K., & Spero, H. J. (2002). Core top calibration of Mg/Ca in tropical foraminifera: Refining paleotemperature estimation. *Geochemistry, Geophysics, Geosystems*, 3(4). <https://doi.org/10.1029/2001GC000200>
- Doss, W., & Marchitto, T. M. (2013). Glacial deep ocean sequestration of CO₂ driven by the eastern equatorial Pacific biologic pump. *Earth and Planetary Science Letters*, 377–378, 43–54. <https://doi.org/10.1016/j.epsl.2013.07.019>
- Eggins, S., De Deckker, P., & Marshall, J. (2003). Mg/Ca variation in planktonic foraminifera tests: Implications for reconstructing palaeoseawater temperature and habitat migration. *Earth and Planetary Science Letters*, 212(3–4), 291–306. [https://doi.org/10.1016/S0012-821X\(03\)00283-8](https://doi.org/10.1016/S0012-821X(03)00283-8)
- Elderfield, H., & Ganssen, G. (2000). Past temperature and $\delta^{18}\text{O}$ of surface ocean waters inferred from foraminiferal Mg/Ca ratios. *Nature*, 405, 25–28. <https://doi.org/10.1038/35013033>
- Emile-Geay, J., & Tingley, M. (2016). Inferring climate variability from nonlinear proxies: Application to palaeo-ENSO studies. *Climate of the Past*, 12, 31–50. <https://doi.org/10.5194/cp-12-31-2016>

- Fairbanks, R. G., Sverdrup, M., Free, R., Wiebe, P. H., & Bé, A. W. H. (1982). Vertical distribution and isotopic fractionation of living planktonic foraminifera from the Panama Basin. *Nature*, 298, 841–844. <https://doi.org/10.1038/298841a0>
- Fairbanks, R. G., & Wiebe, P. H. (1980). Foraminifera and chlorophyll maximum: Vertical distribution, seasonal succession, and paleoceanographic significance. *Science*, 209(4464), 1524–1526. <https://doi.org/10.1126/science.209.4464.1524>
- Faul, K. L., Ravelo, A. C., & Delaney, M. L. (2000). Reconstructions of upwelling, productivity, and photic zone depth in the eastern equatorial Pacific Ocean using planktonic foraminiferal stable isotopes and abundances. *Journal of Foraminiferal Research*, 30(2), 110–125. <https://doi.org/10.2113/0300110>
- Fehrenbacher, J. S., Russell, A. D., Davis, C. V., Spero, H. J., Chu, E., & Höönsch, B. (2018). Ba/Ca ratios in the non-spinose planktic foraminifer Neogloboquadrina dutertrei: Evidence for an organic aggregate microhabitat. *Geochimica et Cosmochimica Acta*, 236, 361–372. <https://doi.org/10.1016/j.gca.2018.03.008>
- Field, D. B. (2004). Variability in vertical distributions of planktonic foraminifera in the California current: Relationships to vertical ocean structure. *Paleoceanography*, 19, PA2014. <https://doi.org/10.1029/2003PA000970>
- Ford, H. L., McChesney, C. L., Hertzberg, J. E., & McManus, J. F. (2018). A deep eastern equatorial Pacific thermocline during the Last Glacial Maximum. *Geophysical Research Letters*, 45, 11,806–11,816. <https://doi.org/10.1029/2018GL079710>
- Ford, H. L., Ravelo, A. C., & Polissar, P. J. (2015). Reduced El Niño–Southern Oscillation during the Last Glacial Maximum. *Science*, 347(6219), 255–258. <https://doi.org/10.1126/science.1258437>
- Giese, B. S., & Ray, S. (2011). El Niño variability in simple ocean data assimilation (SODA), 1871–2008. *Journal of Geophysical Research*, 116, C02024. <https://doi.org/10.1029/2010JC006695>
- Gray, W. R., & Evans, D. (2019). Nonthermal influences on Mg/Ca in planktonic foraminifera: A review of culture studies and application to the Last Glacial Maximum. *Paleoceanography and Paleoclimatology*, 34, 306–315. <https://doi.org/10.1029/2018PA003517>
- Gray, W. R., Weldeab, S., Lea, D. W., Rosenthal, Y., Gruber, N., Donner, B., & Fischer, G. (2018). The effects of temperature, salinity, and the carbonate system on Mg/Ca in Globigerinoides ruber (white): A global sediment trap calibration. *Earth and Planetary Science Letters*, 482, 607–620. <https://doi.org/10.1016/j.epsl.2017.11.026>
- Groeneveld, J., Ho, S. L., Mackensen, A., Mohtadi, M., & Laepple, T. (2019). Deciphering the variability in Mg/Ca and stable oxygen isotopes of individual foraminifera. *Paleoceanography and Paleoclimatology*, 34. <https://doi.org/10.1029/2018PA003533>
- Höönsch, B., Allen, K. A., Lea, D. W., Spero, H. J., Eggins, S. M., Arbuszewski, J., et al. (2013). The influence of salinity on Mg/Ca in planktic foraminifers—Evidence from cultures, core-top sediments and complementary $\delta^{18}\text{O}$. *Geochimica et Cosmochimica Acta*, 121, 196–213. <https://doi.org/10.1016/j.gca.2013.07.028>
- Hughen, K. A., Schrag, D. P., & Jacobsen, S. B. (1999). El Niño during the last interglacial period recorded by a fossil coral from Indonesia. *Geophysical Research Letters*, 26, 3129–3132. <https://doi.org/10.1029/1999GL006062>
- Iida, Y., Kojima, A., Takatani, Y., Nakano, T., Midorikawa, T., & Ishii, M. (2015). Trends in pCO_2 and sea-air CO_2 flux over the global open oceans for the last two decades. *Journal of Oceanography*, 71(6), 637–661. <https://doi.org/10.1007/s10872-015-0306-4>
- Key, R. M., Olsen, A., van Heuven, S., Lauvset, S. K., Velo, A., Lin, X., et al. (2015). Global Ocean Data Analysis Project, Version 2 (GLODAPv2), https://doi.org/10.3334/CDIAC/OTG.NDP093_GLODAPv2
- Khider, D., Stott, L. D., Emile-Geay, J., Thunell, R., & Hammond, D. E. (2011). Assessing El Niño Southern Oscillation variability during the past millennium. *Paleoceanography*, 26, PA3222. <https://doi.org/10.1029/2011PA002139>
- Kiefer, J., & Karanperidou, C. (2019). High-resolution modeling of ENSO-induced precipitation in the tropical Andes: Implications for proxy interpretation. *Paleoceanography and Paleoclimatology*, 217–236. <https://doi.org/10.1029/2018PA003423>
- Koutavas, A., deMenocal, P. B., Olive, G. C., & Lynch-Stieglitz, J. (2006). Mid-Holocene El Niño–Southern Oscillation (ENSO) attenuation revealed by individual foraminifera in eastern tropical Pacific sediments. *Geology*, 34(12), 993–996. <https://doi.org/10.1130/G22810A.1>
- Koutavas, A., & Joanides, S. (2012). El Niño–Southern Oscillation extrema in the Holocene and Last Glacial Maximum. *Paleoceanography*, 27, PA4208. <https://doi.org/10.1029/2012PA002378>
- Lea, D. W., Mashioita, T. A., & Spero, H. J. (1999). Controls on magnesium and strontium uptake in planktonic foraminifera determined by live culturing. *Geochimica et Cosmochimica Acta*, 63(16), 2369–2379. [https://doi.org/10.1016/S0016-7037\(99\)0197-0](https://doi.org/10.1016/S0016-7037(99)0197-0)
- Leduc, G., Vidal, L., Cartapanis, O., & Bard, E. (2009). Modes of eastern equatorial Pacific thermocline variability: Implications for ENSO dynamics over the last glacial period. *Paleoceanography*, 24, PA3202. <https://doi.org/10.1029/2008PA001701>
- Meehl, G. A., Tebaldi, C., Teng, H., & Peterson, T. C. (2007). Current and future U.S. weather extremes and El Niño. *Geophysical Research Letters*, 34, L20704. <https://doi.org/10.1029/2007GL031027>
- Mekik, F. (2018). Do proxies agree? $\delta^{18}\text{O}$, $\delta^{13}\text{C}$ and Mg/Ca from tests of *Neogloboquadrina dutertrei* in the eastern equatorial Pacific. *Geochimica et Cosmochimica Acta*, 236, 260–282. <https://doi.org/10.1016/j.gca.2018.03.005>
- Moy, C. M., Seltzer, G. O., Rodbell, D. T., & Anderson, D. M. (2002). Variability of El Niño–Southern Oscillation activity at millennial timescales during the Holocene epoch. *Nature*, 420, 162–165. <https://doi.org/10.1038/nature01194>
- Nürnberg, D., Bijma, J., & Hemleben, C. (1996). Assessing the reliability of magnesium in foraminiferal calcite as a proxy for water mass temperatures. *Geochimica et Cosmochimica Acta*, 60(5), 803–814. [https://doi.org/10.1016/0016-7037\(95\)00446-7](https://doi.org/10.1016/0016-7037(95)00446-7)
- Ravelo, A. C., & Andreasen, D. H. (1999). Using planktonic foraminifera as monitors of the tropical surface ocean. In F. Abrantes, & A. C. Mix (Eds.), *Reconstructing ocean history* pp 217–243 (pp. 217–243). Boston, MA: Springer. https://doi.org/10.1007/978-1-4615-4197-4_14
- Ravelo, A. C., & Fairbanks, R. G. (1992). Oxygen isotopic composition of multiple species of planktonic foraminifera: Records of the modern photic zone temperature gradient. *Paleoceanography*, 7(6), 815–831. <https://doi.org/10.1029/92PA02092>
- Regenberg, M., Regenberg, A., Garbe-Schönberg, D., & Lea, D. W. (2014). Global dissolution effects on planktonic foraminiferal Mg/Ca ratios controlled by the calcite-saturation state of bottom waters. *Paleoceanography*, 29, 127–142. <https://doi.org/10.1002/2013PA002492>
- Reimer, P. J., Bard, E., Bayliss, A., Beck, J. W., Blackwell, P. G., Ramsey, C. B., et al. (2013). IntCal13 and Marine13 radiocarbon age calibration curves 0–50,000 years cal BP. *Radiocarbon*, 55(4), 1869–1887. https://doi.org/10.2458/azu_js_rc.55.16947
- Rippert, N., Nürnberg, D., Raddatz, J., Maier, E., Hathorne, E., Bijma, J., & Tiedemann, R. (2016). Constraining foraminiferal calcification depths in the western Pacific warm pool. *Marine Micropaleontology*, 128, 14–27. <https://doi.org/10.1016/j.marmicro.2016.08.004>
- Rodbell, D. T., Seltzer, G. O., Anderson, D. M., Abbott, M. B., Enfield, D. B., & Newman, J. H. (1999). An ~15,000-year record of El Niño-driven alluviation in Southwestern Ecuador. *Science*, 283, 516–520. <https://doi.org/10.1126/science.283.5401.516>
- Rongstad, B. L., Marchitto, T. M., & Herguera, J. C. (2017). Understanding the effects of dissolution on the Mg/Ca paleothermometer in planktic foraminifera: Evidence from a novel individual foraminifera method. *Paleoceanography*, 32, 1386–1402. <https://doi.org/10.1002/2017PA003179>

- Rosenthal, Y., & Lohmann, G. P. (2002). Accurate estimation of sea surface temperatures using dissolution-corrected calibrations for Mg/Ca paleothermometry. *Paleoceanography*, 17(3), 1044. <https://doi.org/10.1029/2001PA000749>
- Rustic, G. T., Koutavas, A., Marchitto, T. M., & Linsley, B. K. (2015). Dynamical excitation of the tropical Pacific Ocean and ENSO variability by Little Ice Age cooling. *Science*, 350(6267), 1537–1541. <https://doi.org/10.1126/science.aac9937>
- Sadekov, A., Egging, S. M., De Deckker, P., & Kroon, D. (2008). Uncertainties in seawater thermometry deriving from intratest and intertest Mg/Ca variability in *Globigerinoides ruber*. *Paleoceanography*, 23, PA1215. <https://doi.org/10.1029/2007PA001452>
- Sautter, L. R., & Thunell, R. C. (1991). Planktonic foraminiferal response to upwelling and seasonal hydrographic conditions; sediment trap results from San Pedro Basin, Southern California Bight. *Journal of Foraminiferal Research*, 21(4), 347–363. <https://doi.org/10.2113/gsjfr.21.4.347>
- Scroxton, N., Bonham, S. G., Rickaby, R. E. M., Lawrence, S. H. F., Hermoso, M., & Haywood, A. M. (2011). Persistent El Niño-Southern Oscillation variation during the Pliocene Epoch. *Paleoceanography*, 26, PA2215. <https://doi.org/10.1029/2010PA002097>
- Spero, H. J. (1998). Life history and stable isotope geochemistry of planktonic foraminifera. In R. D. Norris, & R. M. Corfield (Eds.), *Isotope paleobiology and paleoecology* (Vol. 4). Palaeontological Society Papers. Special Publication. <https://doi.org/10.1017/S1089332600000383>
- Steph, S., Regenberg, M., Tiedemann, R., Multizta, S., & Nürnberg, D. (2009). Stable isotopes of planktonic foraminifera from tropical Atlantic/Caribbean core-tops: Implications for reconstructing upper ocean stratification. *Marine Micropaleontology*, 71(1–2), 1–19. <https://doi.org/10.1016/j.marmicro.2008.12.004>
- Takatani, Y., Enyo, K., Iida, Y., Kojima, A., Nakano, T., Sasano, D., et al. (2014). Relationships between total alkalinity in surface water and sea surface dynamic height in the Pacific Ocean. *Journal of Geophysical Research: Oceans*, 119, 2806–2814. <https://doi.org/10.1002/2013JC009739>
- Thirumalai, K., Partin, J. W., Jackson, C. S., & Quinn, T. M. (2013). Statistical constraints on El Niño Southern Oscillation reconstructions using individual foraminifera: A sensitivity analysis. *Paleoceanography*, 28, 401–412. <https://doi.org/10.1002/palo.20037>
- Thunell, R. C., Curry, W. B., & Honjo, S. (1983). Seasonal variation in the flux of planktonic foraminifera: Time series sediment trap results from the Panama Basin. *Earth and Planetary Science Letters*, 64(1), 44–55. [https://doi.org/10.1016/0012-821X\(83\)90051-1](https://doi.org/10.1016/0012-821X(83)90051-1)
- Thunell, R. C., & Reynolds, L. A. (1984). Sedimentation of planktonic foraminifera: Seasonal changes in species flux in the Panama Basin. *Micropaleontology*, 243–262. <https://doi.org/10.2307/1485688>
- Tudhope, A. W., Chilcott, C. P., McCulloch, M. T., Cook, E. R., Chappell, J., Ellam, R. M., et al. (2001). Variability in the El Niño-Southern Oscillation through a glacial-interglacial cycle. *Science*, 291. <https://doi.org/10.1126/science.1057969>
- White, S. M., Ravelo, A. C., & Polissar, P. J. (2018). Dampened El Niño in the early and mid-Holocene due to insolation-forced warming/deepening of the thermocline. *Geophysical Research Letters*, 45, 316–326. <https://doi.org/10.1002/2017GL075433>
- Wilk, M. B., & Gnanadesikan, R. (1968). Probability plotting methods for the analysis of data. *Biometrika*, 55(1), 1–17. <https://doi.org/10.1093/biomet/55.1.1>
- Zhu, J., Liu, Z., Brady, E., Otto-Bliesner, B., Zhang, J., Noone, D., et al. (2017). Reduced ENSO variability at the LGM revealed by an isotope-enabled Earth system model. *Geophysical Research Letters*, 44, 6984–6992. <https://doi.org/10.1002/2017GL073406>

References From the Supporting Information

- Druffel, E. M. (1981). Radiocarbon in annual coral rings from the eastern tropical Pacific Ocean. *Geophysical Research Letters*, 8(1), 59–62. <https://doi.org/10.1029/GL008i001p00059>
- Jones, K., Hodgins, G., Dettman, D., Andrus, C., Nelson, A., & Etayo-Cadavid, M. (2007). Seasonal variations in Peruvian marine reservoir age from Pre-Bomb *Argopepon Purpuratus* shell carbonate. *Radiocarbon*, 49(2), 877–888. <https://doi.org/10.1017/S0033822200042740>
- Parnell, A. C., Haslett, J., Allen, J. R. M., Buck, C. E., & Huntley, B. (2008). A flexible approach to assessing synchronicity of past events using Bayesian reconstructions of sedimentation history. *Quaternary Science Reviews*, 27(19–20), 1872–1885. <https://doi.org/10.1016/j.quascirev.2008.07.009>
- Petchey, F., Phelan, M., & White, J. P. (2004). New ΔR values for the Southwest Pacific Ocean. *Radiocarbon*, 46(2), 1005–1014. <https://doi.org/10.1017/S0033822200036079>
- Stuiver, M., & Reimer, P. (1993). Extended ^{14}C data base and revised CALIB 3.0 ^{14}C age calibration program. *Radiocarbon*, 35(1), 215–230. <https://doi.org/10.1017/S0033822200013904>
- Stuiver, M., Reimer, P., Bard, E., Beck, J., Burr, G., Hughen, K., et al. (1998). INTCAL98 radiocarbon age calibration, 24,000–0 cal BP. *Radiocarbon*, 40(3), 1041–1083. <https://doi.org/10.1017/S0033822200019123>
- Taylor, R. E., & Berger, R. (1967). Radiocarbon content of marine shells from the Pacific coasts of Central and South America. *Science*, 158(3805), 1180–1182. <https://doi.org/10.1126/science.158.3805.1180-a>